Measuring and monitoring heavy-oil reservoir properties

KEVIN WOLF, TIZIANA VANORIO, and GARY MAVKO, Stanford University, Stanford, USA

The level of interest in heavy-oil and bitumen reservoirs has dramatically increased in recent times, stimulating research on their properties under various conditions. Rock physics provides the crucial link between the physical properties of the reservoir and seismic properties that can be remotely measured; however, there is currently no robust model to predict or infer the properties of heavy-oil or bitumen sands from seismic data, nor is there sufficient experimental data to calibrate such models. This is due to the particularly challenging nature of experimental measurements of heavy-oil sands.

We present the approach we have taken in our laboratory to solve some of these problems, and discuss the hurdles that must be addressed to fully characterize these complex rocks.

We show a methodology to characterize and monitor heavy-oil reservoirs by inverting converted-wave seismic data in order to obtain P-to-S converted-wave elastic impedance, or PSEI, estimates as a function of angle. By examining these data in "PSEI space" (crossplots of PSEI values obtained at different angles), we can infer the conditions in the reservoir.

We then present the design of our ultrasonic pulse transmission transducers. These transducers are designed specifically to overcome some of the problems encountered when measuring the ultrasonic acoustic and elastic properties of heavy-oil saturated sands at elevated temperatures and pressures.

Converted P-to-S wave elastic impedance (PSEI)

PSEI was defined by Gonzalez et al. (2003) as:

$$PSEI(\theta_P) = \rho^{c} Vs^{d} \tag{1}$$

where

$$c = \frac{K \sin\theta_P}{\sqrt{\frac{1}{K^2} - \sin^2\theta_P}} \left(2\sin^2\theta_P - \frac{1}{K^2} - 2\cos\theta_P \sqrt{\frac{1}{K^2} - \sin^2\theta_P} \right) \tag{2}$$

$$d = \frac{4K \sin\theta_P}{\sqrt{\frac{1}{K^2} - \sin^2\theta_P}} \left(\sin^2\theta_P - \cos\theta_P \sqrt{\frac{1}{K^2} - \sin^2\theta_P} \right) \tag{3}$$

K is the average V_S/V_P, θ_P is the incident P-wave angle at the conversion point, and ρ is the density. Analyzing the behavior of exponents c and d reveals that at small incidence angles both V_S and ρ contribute to the PSEI value. However, at larger angles, density begins to dominate, and this allows separation of density and shear-wave velocity trends in PSEI space.

Figure 1 shows an example of this separation for a hypothetical situation in a well. The original well-log data are in black. The data were systematically altered to reveal the shear-wave velocity and density trends. Warm colors (red to yellow) reveal the V_S trend as V_P is decreased to 50% of its original value in 10% decrements. Similarly, cool colors (green to blue) reveal the density trend as density is decreased to 75% of its original value by 5% decrements. The ability to discriminate between these two trends is important for heavy-oil reservoirs since they are commonly produced via steam injection. As a reservoir is heated, the shear velocity of the heavy-oil sand decreases dramatically, and at the point of injection steam will begin to displace the heavy oil in the pore space which will decrease the reservoir density in that area. We can

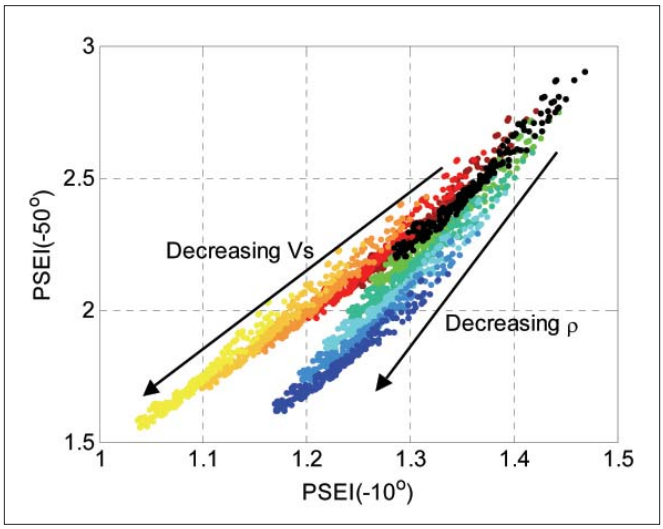

Figure 1. *Crossplot of near-angle PSEI (-10°) versus far-angle PSEI (-50°) for a well log from a bitumen reservoir. The original well-log data are in black. Warm colors represent changing shear-velocity measurements by decrements of 10% to a minimum of 50% of their original value. Cool colors represent changing density measurements by decrements of 5% to a minimum of 75% of their original value.*

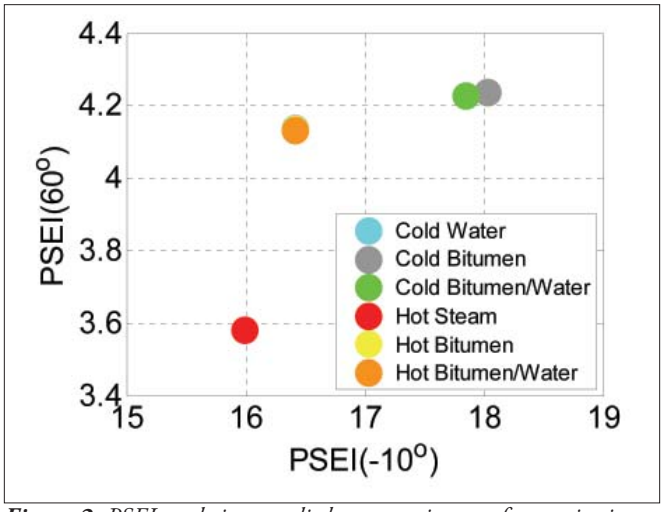

Figure 2. *PSEI analysis as applied to reservoir states for monitoring heated zones and steam chambers. Note that cold water and hot bitumen data points are mostly obscured by the hot bitumen/water data point.*

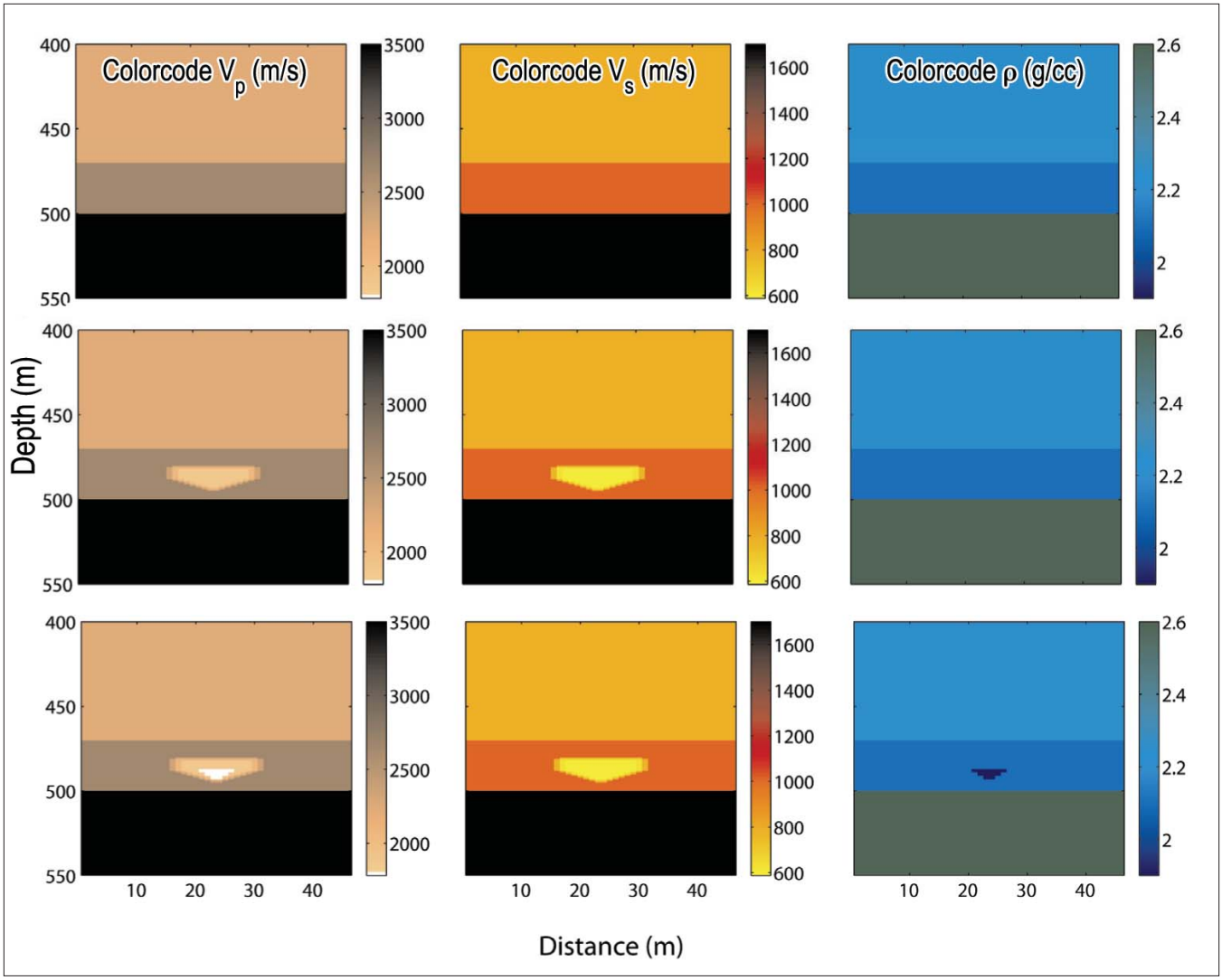

Figure 3. *Synthetic Earth models for cold reservoir (top), heated reservoir (middle), and heated reservoir with steam chamber (bottom). The shale overburden and limestone basement rock are the same in all cases, and the reservoir is at a depth of 470-500 m. The P-wave velocity is shown in the first column, S-wave velocity in the middle column, and density in the right column.*

identify these trends with PSEI and use this knowledge to help characterize and monitor the production of thermally produced heavy oil sands.

This is illustrated in Figure 2 which shows where various synthetic reservoir states plot in PSEI space. These reservoir states show that discriminating between cold bitumen-bearing zones, heated bitumen-bearing zones, and steam-saturated zones is possible in PSEI space provided both near- and far-angle PSEI attributes can be determined.

PSEI inversion for reservoir characterization and monitoring

To illustrate the utility of PSEI for characterization, we have created a simple three-layer synthetic Earth model. It consists of a uniform shale unit overlying a 30-m reservoir interval (at a depth of 470-500 m) which is in turn underlain by a uniform limestone basement. Inversion has been performed on the reservoir when it is in three distinct states: the original cold reservoir, the reservoir containing a heated zone that is 15 m wide and 15 m thick at its widest and thickest portions, and the reservoir containing the same heated zone as well as a steam-saturated zone that is 6 m wide and 6 m thick across its widest and thickest dimensions.

Figure 3 shows the distribution of reservoir properties for each reservoir state. Converted-wave synthetic seismic data were then computed through the Earth models using a 125-Hz Ricker wavelet at offsets corresponding to P-wave incidence angles of 10 and 50° at the top of the reservoir. The inversion itself was model-based with the initial model for each inversion created from three "wells"—one on each end of the Earth model and one at its center. In order to build a model consistent with the converted-wave seismic, the wells must first be converted to pseudo-wells as proposed by Gonzales et al. (2004). These pseudo-wells are then used to build the initial model, and the model-based inversion can be carried out.

The results of the inversion at 10° (left column) and 50° (right column) are shown for the three Earth models in Figure 4. The results from the cold reservoir 10° inversion (top left) clearly show the top and bottom of the reservoir. However, the base of the reservoir is poorly resolved in the 50° data.

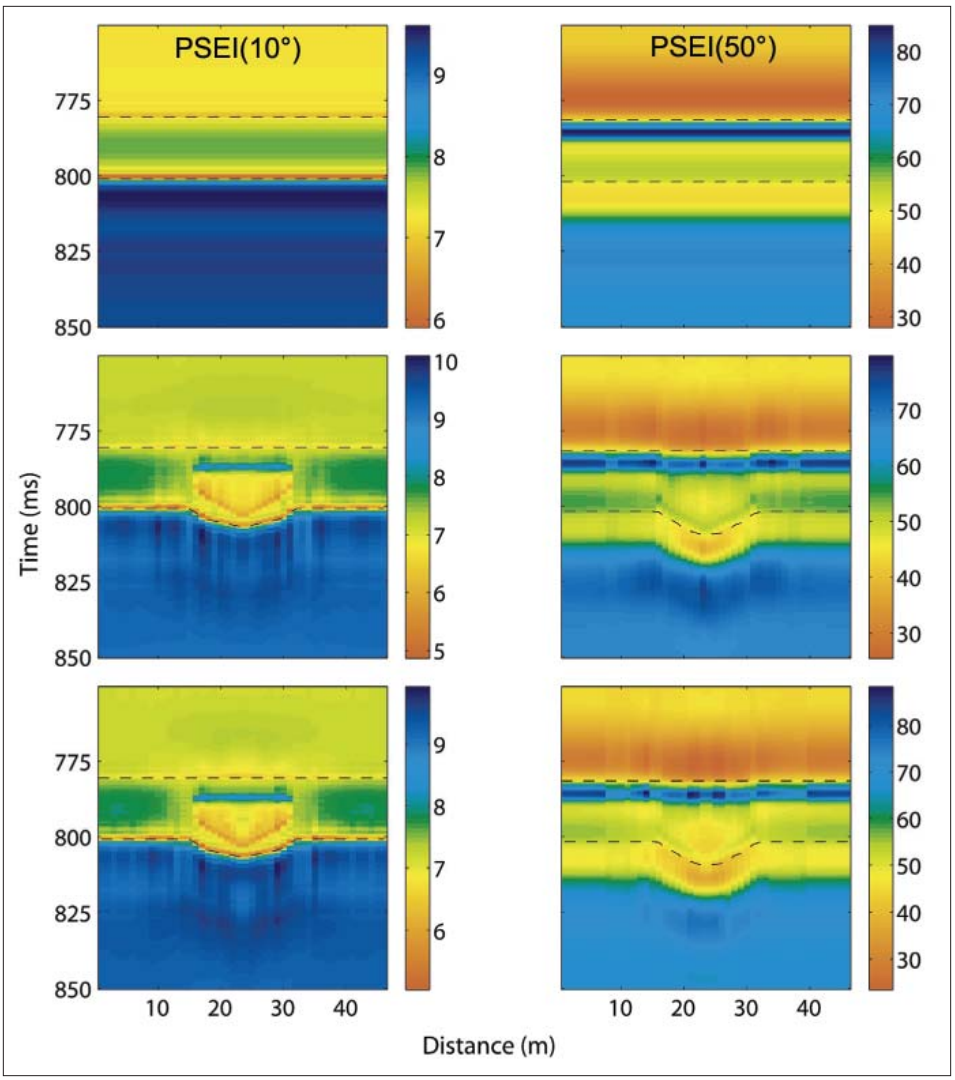

Figure 4. *Inversion results for cold reservoir (top), heated reservoir (middle), and heated reservoir with steam chamber (bottom). The left column shows the 10° inversion and the right column the 50° inversion. Dashed black lines show the top and bottom of the reservoir as picked from the synthetic seismic sections.*

This is due to the character of the seismic data at the reservoir-limestone interface. The angle of incidence for this case is postcritical, and the resulting low-amplitude reflections are not sufficient for the inversion to clearly resolve the boundary between the reservoir and the limestone basement. Similar patterns with regards to incident angle can be seen in the inversion results from the heated reservoir (middle row). Again, the 50° inversion does not adequately define the base of the reservoir. However, on the 10° inversion, the top and base of the reservoir are delineated, and the heated zone is clearly visible and correctly located. At 50° the inversion no longer sees the heated zone in the reservoir; however, this is not unexpected. As the angle is increased, the sensitivity of PSEI to shear-wave velocity is decreased, and the sensitivity to density is increased. Since the heated reservoir only contains contrasts in the shear-wave velocity, it should appear homogeneous at far offsets. For the heated reservoir with steam chamber (bottom row), the 10° inversion again clearly defines the heated zone. Also, the 50° inversion shows a low-impedance zone in the heated zone which corresponds to the location of the steam chamber. This is the result of the density contrast created by steam replacing bitumen in the pore space.

These results are very encouraging and demonstrate that the proposed methodology can provide a robust method for tracking heated zones within a bitumen reservoir and the formation of steam chambers when good quality converted-wave seismic data are available.

However, there are also some artifacts in the inversion which must be taken into account when interpreting the results. One is the high-impedance zone directly overlying the heated reservoir in the 10° inversion. This is likely a result of wavelet effects, tuning, or possibly related to the limited frequency content of the inversion. Also, real seismic data will have a lower signal-to-noise ratio than our idealized synthetic case which will have an effect on the quality of the inversion.

Data in PSEI space

To fully realize the utility of the inversion, it is necessary to plot the data in PSEI space (Figure 5). A realistic way of looking at the data is to imagine them as being snapshots of a reservoir at different times during production. The cold reservoir (Figure 5a) is representative of the untouched reservoir before production has commenced. There is a clear separation in data points that correspond to the overlying shale (magenta), underlying limestone (green), and the reservoir interval (blue).

The next snapshot (Figure 5b) corresponds to the reservoir after steam has been injected to stimulate production. Heating the reservoir reduces the shear modulus of the bitumen, which in turn lowers the shear-wave velocity in the heated zone. As expected, the heated reservoir points (red) shift to the left in PSEI space, indicating that the reservoir zones corresponding to those data points have been heated. Note that some blue data points also have migrated in the same direction. This is because the seismic inversion tends to smear boundaries between different zones instead of providing an extremely sharp boundary. Also, the models themselves have a transition between reservoir properties instead of a sharp boundary.

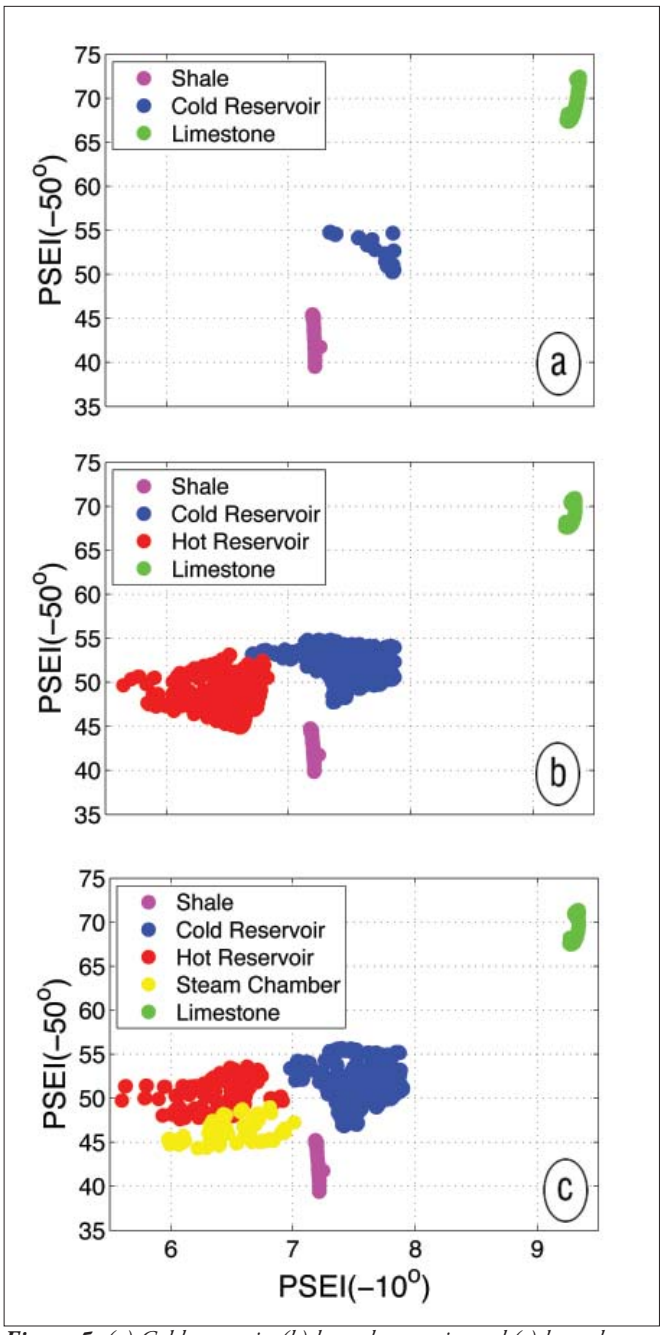

Figure 5. *(a) Cold reservoir, (b) heated reservoir, and (c) heated reservoir with results of steam chamber inversion plotted in PSEI space.*

The next snapshot (Figure 5c) is after the formation of a steam chamber around the injection point. The effect of this is to lower the density of the reservoir in the steam chamber zone, as well as decreasing the P-wave velocity. As density decreases, we expect data points to migrate downward in PSEI space. This can be seen in Figure 5c where the distribution of data points corresponding to the steam chamber (yellow) generally plots below those in the heated zone (red). This is encouraging; however, there is some overlap in the location of the yellow points in Figure 5c and the location of heated data points in Figure 5b. This suggests that the formation of a steam chamber may not be sufficient to clearly delineate data points corresponding to heated reservoir zones and those to steam-filled reservoir zones. However, the relative distribution of the points corresponding to the heated and steam-filled zones does allow determination of which data points, and hence which reservoir zones, are more likely to be steam-saturated. Also, if the size of the steam chamber grows larger in dimension than in this example, the effect of smearing the boundaries in the inversion will be less pronounced, which may allow clearer distinction between heated and steam-saturated sections of the reservoir.

Laboratory measurements of heavy-oil reservoirs

The preceding inversion example shows the possibilities that exist for using PSEI to monitor thermal production. However, without robust rock physics models to link the observed data to the physical properties of the reservoir, these results can only be used for qualitative descriptions of the reservoir.

Thus, we need a massive set of robust laboratory measurements of the general properties, including acoustic and elastic properties of bitumen and heavy-oil sands to establish well-defined rock physics relationships for these materials.

A great deal of research has been done on room temperature measurements of the properties of hard rocks (sandstones, carbonates, etc.) to establish empirical and theoretical relationships between a number of rock properties. Despite their inherent complexities, these hard rocks are, for several reasons, typically much simpler to measure than bitumen sands. Hard rocks have a high impedance and higher quality factor than the soft sediments that typically make up bitumen reservoirs. The relatively low impedance and quality factor of bitumen sand samples make it more difficult to obtain large-amplitude P- or S-wave signals through them. In addition, bitumen sands are generally poorly consolidated and bound together by the bitumen filling the pore space; this leads to properties that can vary quite drastically after heating. These characteristics make the measurement of bitumen sand velocities via ultrasonic pulse transmission experiments particularly challenging.

To attempt to overcome these challenges, we have designed a unique ultrasonic pulse transmission system specifically for measurements in bitumen sands. The system has many unique features, and in this article we will focus on what we consider the most crucial element—the transducers.

Transducer design

Traditionally, ultrasonic velocity measurements have been made with high-impedance end-caps with minimal effort put into the design of the transducers themselves. This has not been a major impediment because the majority of rock physics measurements have been made on hard rocks, such as sandstones, carbonates, and some shales whose properties are not as variable as unconsolidated sediments, especially unconsolidated sediments that are fixed by bitumen. Our work has paid particular attention to the design of the transducers to ensure that the best signal possible is recorded under all conditions.

Basic transducer design must take into account all vital

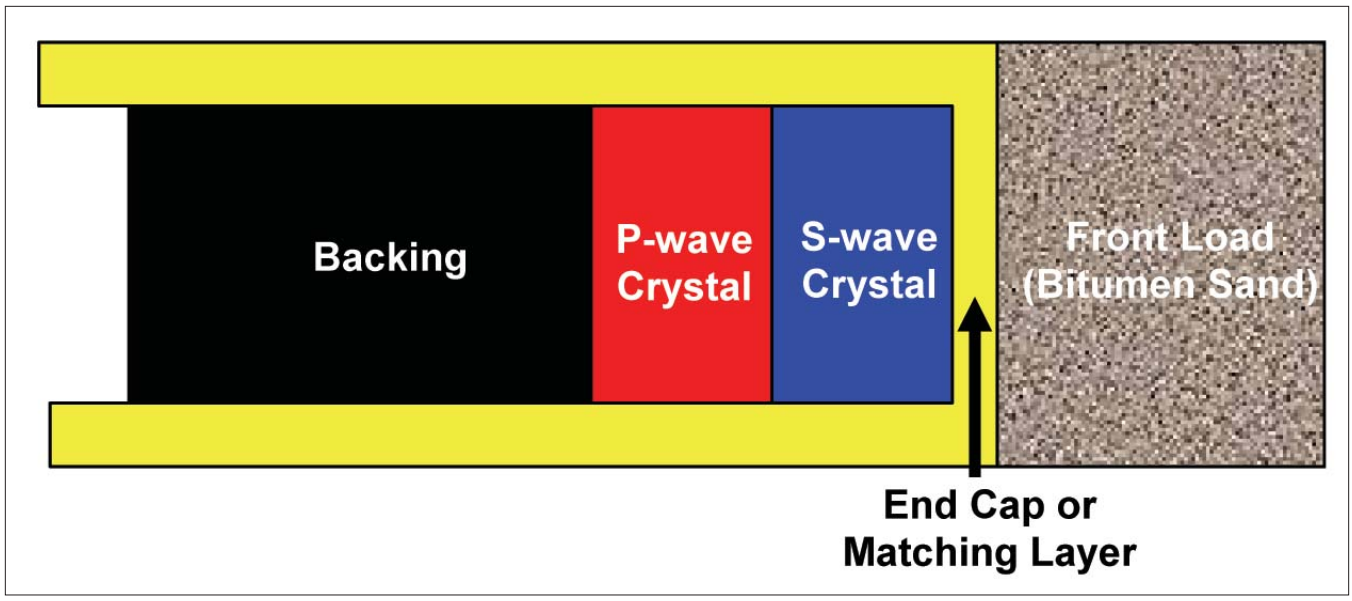

Figure 6. *The generalized transducer model consists of a crystal backing, two piezoelectric crystals (one to generate P-waves and one to generate S-waves), an end cap or matching layer, and the load.*

elements: the piezoelectric crystal (or crystals for generating multiple wave types or polarizations), the backing behind the crystals, the end cap or matching layer between the crystals and the load, and the load that the generated waves will travel through.

Figure 6 illustrates a general schematic for an ultrasonic transducer with two piezoelectric crystals—one to generate P-waves and one to generate S-waves. In order to make the design optimum, a transducer modeling code, which utilizes the KLM equivalent circuit (Krimholtz et al., 1970), has been written to measure the response of the transducer given different transducer and sample properties. The KLM model easily allows any number of piezoelectric crystals, matching layers, etc. to be added into the transducer model. This allows modeling many types of transducers, including those with multiple crystals for making anisotropic measurements, etc. The ABCD matrix representation of the individual components and loads in the KLM model is also used. Each component of the KLM model can be represented as a two-port network, which can then be characterized using matrix methods (Ramo et al., 1984). This formulation allows the input/output voltage and current in each component to be related through a 2×2 matrix. Then, in order to calculate the response of the entire transducer, the entire chain of matrices is multiplied together, which relates the input voltage and current to the output force and velocity from the transducer. This matrix representation makes calculating the transducer response fast and easier to code.

The responses of various transducer designs, under various conditions are shown in Figure 7. The effect of varying the end-cap or matching layer material is shown in Figure 7a. Traditional hard rock transducers use stainless steel end caps. For hard rock samples, this does not create a large mismatch in impedance between the transducer and the sample since the sample itself has high impedance. However, when dealing with unconsolidated or other soft samples, a high-impedance end cap creates a large impedance contrast between the transducer and the samples, resulting in less energy being transferred to the sample. Zimmer (2003) attempted to overcome these problems for measurements on unconsolidated sands by using a glass-filled polycarbonate end cap. This impedance of this type of end cap is more similar to unconsolidated sand than traditional steel end caps. However, this material cannot withstand the elevated temperatures (200°C) needed for our experiment. The choice was made to use Torlon end caps because Torlon has low impedance similar to that of unconsolidated sand, and its properties are reasonably stable with temperature. Figure 7a shows the impulse response of the transducer at room temperature with two different end cap materials. The traditional steel end cap is blue, and the Torlon end cap is red. Figure 7b shows the exact same transducer, and the modeled response at elevated temperatures is also shown. Clearly the Torlon provides a cleaner, higher-amplitude signal than stainless steel in this case, especially for the shear wave.

Another important consideration is the thickness of the end cap or matching layer which, ideally, should be precisely one quarter of a wavelength. This ensures that any reflected energy will constructively interfere and lead to the best possible impulse response of the system at the frequency at which it is designed to operate. However, in this case both compressional and shear waves need to be generated, and each wave type has its own wavelength. Thus, a compromise must be reached between the two ideal thicknesses for each wave. As can be seen in Figure 7c, a thickness of $2.54e^{-3}$ m provides a large-amplitude, broadband impulse response. If the thickness is increased or decreased, the impulse response is adversely affected. For increased thickness, in blue, the first arrival of the shear wave is not as prominent. In addition, the maximum amplitude is slightly decreased.

The backing material also has a large effect on the im-

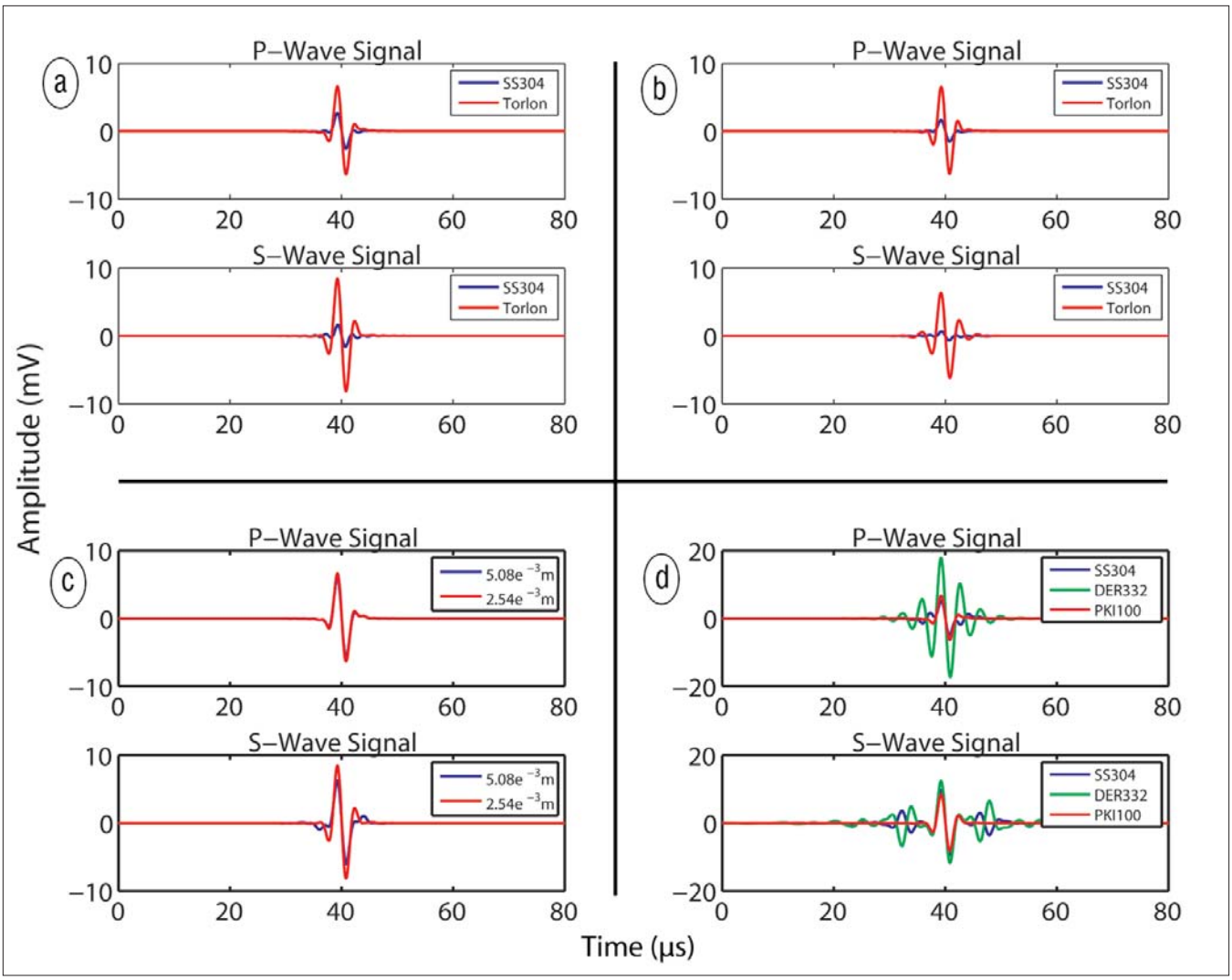

Figure 7. *The effect of varying transducer properties on the generated signal. (a) Varying end-cap material at room temperature, stainless steel in blue and Torlon in red. (b) Varying end-cap material at elevated temperature, stainless steel in blue and Torlon in red. (c) Varying Torlon end-cap thickness. (d) Varying backing material used, stainless steel in blue, Dow Epoxy Resin 332 in green, and lead metaniobate in red.*

pulse response of the transducer. Ideally the backing should be a very lossy and high-impedance material compared to the crystals used to generate the signal. The high impedance will ensure that energy radiating out the back of the crystal is mostly reflected back into the sample. The backing also needs to be very lossy so that any energy transmitted into the backing does not reflect off the rear of the backing and adversely affect the signal.

One procedure for producing high-impedance lossy backings is to combine tungsten and epoxy to obtain the desired characteristics. However, this poses several difficulties for our system. The first is that the epoxy is not able to withstand elevated temperatures. The second is that both the P- and S-wave impedances need to be matched to specific values which would involve much time-consuming research to get the correct proportions and impedances. To overcome these problems, we used the same piezoelectric material for the backing that is employed for the crystal. This ensures that the backing has the correct matching impedance for both the P- and S-waves.

Figure 7d compares the impulse response for three transducers which are identical except for the backing. It is immediately obvious that the most broadband transducer is the one with the perfectly matched backing of lead metaniobate. It will be easiest to clearly identify the first arrival of this signal given the clear first break on both the P- and S-wave impulse response. It is also apparent that the perfectly matched backing has lower overall amplitude. This is because the energy leaving the back of the piezoelectric crystal is not reflected back by the backing. Although this is not necessarily desirable, the clean nature of the signal makes up for the loss in amplitude.

Also, it is important to keep in mind that the backing is not lossy in any of the three cases presented in Figure 7d. This means that any energy passed into the backing will reflect off the rear of the backing and interfere with the desired signal. An easy way to overcome this problem is to ensure that the backing is sufficiently long so that the reflected wave will not arrive at the far end of the sample before the first break of the desired signal. Our final design includes this consideration.

The frequency at which the measurements are made has also been modified from traditional ultrasonic transducers used for consolidated rocks. 250-kHz broadband piezoelectric crystals are used instead of standard 1-MHz crystals; this reduced energy absorption and scattering as the signals pass through the samples (Zimmer, 2003). Also, using a frequency of 250 kHz ensures that we will have at least one wavelength within our samples in order to obtain robust measurements.

Summary

A methodology using PSEI attributes has been developed for characterizing and monitoring bitumen reservoirs undergoing thermal production. The example shown demonstrates the ability of the method to discriminate between nonreservoir and reservoir rocks, as well as zones within the reservoir that have been heated or have had reservoir fluids replaced by steam. The lack of a well-defined rock physics model or transform for heavy-oil or bitumen sands currently precludes quantitative interpretation. However, with equipment specifically designed for heavy oil, we can accrue that data needed for such a model.

Suggested reading. "Near and far offset P-to-S elastic impedance for discriminating fizz water from commercial gas" by Gonzalez et al. (*TLE*, 2003). "A practical procedure for P-to-S 'elastic' impedance (PSEI) inversion: Well log and synthetic seismic examples for identifying partial gas saturations" by Gonzalez et al. (SEG 2004 *Expanded Abstracts*). "New equivalent circuits for elementary piezoelectric transducers" by Krimholtz et al. (*Electronics Letters*, 1970). More on the ABCD matrix representation of two-port networks can be found in *Fields and Waves in Communications Electronics* by Ramo et al. (Wiley, 1984). Seismic Velocities in Unconsolidated Sands: Measurements of Pressure, Sorting and Compaction Effects by Zimmer (PhD thesis, Stanford University, 2003). TLE

Corresponding author: kxwolf@stanford.edu